MINISTRY OF EDUCATION
AND TRAINING

VIETNAM ACADEMY
OF SCIENCE AND TECHNOLOGY

GRADUATE UNIVERSITY SCIENCE AND TECHNOLOGY

Nguyen Thi Thu Hien

STUDY ON THE CHEMICAL CONSTITUENTS AND INHIBITORY ACTIVITIES AGAINST α-GLUCOSIDASE AND XANTHINE OXIDASE OF *GLINUS OPPOSITIFOLIUS* (L.) A. DC., MOLLUGINACEAE

SUMMARY OF THE DOCTORAL DISSERTATION IN MATERIALS SCIENCE

Major: Organic Chemistry

Code: 9440114

Ho Chi Minh city - 2026

The thesis was completed at: Graduate University Science and Technology - Vietnam Academy of Science and Technology

Supervisors:

Supervisors 1: Assoc. Prof. Dr. Le Tien Dung, Institute of Advanced Technology

Supervisors 2: Assoc. Prof. Dr. Nguyen Trong Tuan, Can Tho Univeristy

Referee 1: Assoc. Prof. Dr. Nguyen Quang Vinh

Referee 2: Assoc. Prof. Dr. Tran Ngoc Quyen

The dissertation is examined by Examination Board of Graduate University of Science and Technology, Vietnam Academy of Science and Technology at 20 / 01/ 2026

The dissertation can be found at:

1. Graduate University of Science and Technology Library
2. National Library of Vietnam

LIST OF THE PUBLICATIONS
RELATED TO THE DISSERTATION

1. Nguyen Thi Thu Hien, Huynh Tran Quoc Dung, Bui Hoang Minh, Tran Van Chen, Nguyen Trong Tuan, Le Tien Dung, 2023, A New Flavonoid Derivative and Inhibitory Effects on Xanthine Oxidase and α-glucosidase from *Glinus oppositifolius*, Current Organic Chemistry, 27(5), pp. 1371-1379.
2. Nguyen Thi Thu Hien, Dung Huynh Tran Quoc, Phuong Vu Luu, Tuan Nguyen Trong, Dung Le Tien, 2025, Acylamino Acid from Aerial Parts of *Glinus oppositifolius* Aug. DC. and Its Xanthine Oxidase, α-glucosidase Inhibitory Activities, Natural product research, 15(9), pp. 1-14
3. Nguyen Thi Thu Hien, Dung Huynh Tran Quoc, Chen Tran Van, Tran Le Viet Ha, Tuan Nguyen Trong, Dung Le Tien, 2025, Characterization of a Novel Triterpenoid Saponin from *Glinus oppositifolius* Aerial Parts with Enzyme Inhibitory Potential, Current Organic Chemistry, 27(7), pp. 624-629

INTRODUCTION

1. Necessity of research

Xanthine oxidase (XO) catalyzes the oxidation of hypoxanthine to xanthine and uric acid in purine metabolism. Inhibiting XO is thus considered an effective strategy for treating hyperuricemia and disorders related to reactive oxygen species (ROS). Epidemiological studies have revealed a strong link between gout and diabetes mellitus, both major risk factors for cardiovascular diseases and mortality. Diabetes, a chronic metabolic disorder marked by high blood glucose due to impaired insulin function, currently affects nearly 12% of the global population, emphasizing the need for effective therapies.

Natural products have gained attention as potential alternatives owing to their broad pharmacological effects and lower toxicity. *Glinus oppositifolius* (L.) A. DC. (Rau đắng đất), a medicinal plant common in southern Vietnam, exhibits various biological activities, including immunomodulatory, hepatoprotective, antibacterial, antihyperlipidemic, antihyperglycemic, and antioxidant effects. However, data on its XO and α-glucosidase inhibitory activities remain limited.

Recently, network pharmacology has provided a powerful approach to exploring multi-target mechanisms and improving therapeutic efficacy. Yet, the bioactive components and molecular mechanisms underlying the antidiabetic and antigout potential of *G. oppositifolius* have not been examined using this method. Therefore, this study, entitled “Study on the chemical constituents and inhibitory activities against *α*-glucosidase and xanthine oxidase of *Glinus oppositifolius* (L.) A. DC.,

Molluginaceae", aims to identify natural bioactive compounds and elucidate their mechanisms to enhance the medicinal value and ethnopharmacological understanding of this Vietnamese plant.

2. Research objectives of the thesis

- Evaluated the inhibitory effects of the fractionated extracts on α-glucosidase and xanthine oxidase enzymes.
- Isolated, purified, and elucidated the structures of several compounds exhibiting α-glucosidase and xanthine oxidase inhibitory activities from *Glinus oppositifolius*.
- Assessed the α-glucosidase and xanthine oxidase inhibitory activities of the isolated compounds.
- Analyzed and predicted the potential mechanisms of Glinus oppositifolius in the treatment of type 2 diabetes mellitus and gout using network pharmacology and molecular docking approaches.

3. Main research contents of the thesis

- Extracted and prepared the crude extract as well as the fractionated extracts from *Glinus oppositifolius*.
- Investigated the α-glucosidase and xanthine oxidase inhibitory activities of the fractionated extracts.
- Isolated and purified bioactive compounds from the most active fractions.
- Elucidated the chemical structures of the purified isolated compounds.
- Evaluated the α-glucosidase and xanthine oxidase inhibitory activities of the purified compounds.

- Conducted network pharmacology analysis to explore the potential mechanisms of *Glinus oppositifolius* in the treatment of type 2 diabetes mellitus and gout, and performed molecular docking studies between key bioactive compounds and potential target proteins.

CHAPTER 1. OVERVIEW

1.1. Overview of Diabetes Mellitus

Diabetes mellitus is a heterogeneous metabolic disorder characterized by chronic hyperglycemia resulting from defects in insulin secretion, insulin action, or both. Prolonged hyperglycemia can lead to disturbances in the metabolism of carbohydrates, lipids, and proteins, and may cause damage to various organs, particularly the heart and blood vessels, eyes, nervous system, and kidneys.

1.2. Tổng quan về bệnh Gout

Gout, also known as gouty arthritis, is a metabolic disorder of purine metabolism that results in elevated levels of uric acid in the blood. The accumulation of monosodium urate crystals occurs in various tissues, including synovial membranes, articular cartilage, tendons, and subcutaneous tissues. The disease is characterized by recurrent episodes of acute arthritis, which often cause severe pain and may progress to chronic arthritis if left untreated.

1.3. Overview of *Glinus oppositifolius*

1.3.1. Botanical Description

Glinus oppositifolius (L.) A. DC. is an annual herb with slender, prostrate, hairy stems that are green when young and turn rigid, reddish-brown with swollen nodes at maturity. The plant has a

distinctly bitter taste. Leaves are simple and arranged in whorls. Inflorescences arise from leaf axils, each bearing 3–6 small, bisexual, petal-less flowers with five sepals and stamens. The fruit is a three-loculed capsule containing numerous small, reddish-brown, reniform seeds with reticulate surfaces and appendages at the hilum.

1.3.2. Chemical constituents

Phytochemical investigations have revealed that Glinus oppositifolius contains diverse classes of secondary metabolites, including flavonoids, triterpenoid saponins, aromatic compounds, steroids, acylamino acid derivatives, nucleosides, and several other constituents. Among these, flavonoids and triterpenoid saponins are the predominant components and have been demonstrated to exhibit a wide range of pharmacological activities in various experimental models.

1.3.3. Pharmacological activities

Numerous studies have reported that *Glinus oppositifolius* possesses various pharmacological properties, including antioxidant, hepatoprotective, antibacterial, analgesic, anti-inflammatory, antifungal, antimalarial, anticancer, antihyperglycemic, antihyperlipidemic, sedative, and anxiolytic effects.

1.4. Overview of Network Pharmacology and Molecular Docking

Network pharmacology is an interdisciplinary approach that integrates principles from molecular biology, biochemistry, and bioinformatics. It has gained increasing attention due to its high success rate in clinical trials, reduced side effects, cost-

effectiveness, and ability to enhance drug efficacy. Network pharmacology enables the modulation of signaling pathways through multiple channels and allows the simultaneous targeting of multiple genes and proteins associated with disease mechanisms.

Molecular docking, on the other hand, is the study of how two or more molecular structures—such as drugs, enzymes, or proteins—fit and interact with each other. It is a computational modeling technique used to predict the binding mode and interaction between a protein (enzyme) and small molecules, thereby providing insights into the molecular basis of drug action and facilitating the design of potential therapeutic agents.

CHAPTER 2. OBJECTS AND METHODOLOGY

2.1. Research objects

The aerial parts of *Glinus oppositifolius* were collected in Tây Ninh Province, Vietnam, in April 2022. The plant material was taxonomically identified by Dr. Nguyễn Thụy Vy, Faculty of Biology and Biotechnology, University of Science, Ho Chi Minh City.

2.2. Research methods

2.2.1. Extraction and Fractionation

Fresh *Glinus oppositifolius* (31 kg) was air-dried and ground into coarse powder (8.0 kg). The powdered material was exhaustively macerated at room temperature with 70% ethanol (30 L × 4 times). The combined ethanolic extracts were concentrated under reduced pressure to yield a crude ethanolic extract (9 L). This extract was successively partitioned with ethyl acetate (EtOAc, 9 L × 5 times), and the combined EtOAc

layers were concentrated under reduced pressure to obtain an EtOAc fraction (78 g). The remaining aqueous layer was further partitioned with *n*-butanol (*n*-BuOH, 9 L × 7 times) and concentrated under reduced pressure to yield an *n*-BuOH fraction (117 g).

2.2.2. Isolation of Compounds

The ethyl acetate extract (60 g) was separated by silica gel column chromatography with a $CHCl_3$/MeOH gradient (100:0 → 60:40, v/v), yielding nine fractions (E1–E9). Fraction E1 (15.9 g) was further chromatographed using $CHCl_3$/EtOAc (80:20 → 50:50, v/v) to obtain seven subfractions (E1.1–E1.7). From these, subfraction E1.2 produced **G-20** (10 mg) after CH_2Cl_2/MeOH elution and recrystallization, while E1.4 and E1.5 afforded **G-13** (18 mg) and **G-14** (13 mg), respectively.

Fractions E2 (0.96 g) and E3 (1.65 g) were purified on Sephadex LH-20 with MeOH to yield **G-8** (13 mg), **G-16** (20 mg), **G-2** (52 mg), and **G-18** (16 mg). Fraction E4 (17.01 g) was separated on a C18 column using a MeOH/H_2O gradient (0:100 → 22:78, v/v) to give five subfractions. Among them, E4.1 provided **G-19** (20 mg) after Sephadex LH-20 purification, while E4.2, E4.4, and E4.5 yielded **G-3** (50 mg), **G-4** (15 mg), and **G-5** (19 mg) after crystallization from MeOH.

Fraction E5 (8.42 g) was further fractionated on Sephadex LH-20 to give three subfractions (E5.1–E5.3). Recrystallization and preparative LC yielded **G-9** (15 mg), **G-7** (12 mg), and **G-10** (20 mg), respectively.

The *n*-butanol extract (90 g) was fractionated on a silica gel column using a $CHCl_3$/MeOH gradient (95:5 → 40:60, v/v) to yield eight fractions (B1–B8). Fraction B3 (7 g) was further separated with $CHCl_3$/EtOAc (90:10 → 50:50, v/v) into six subfractions (B3.1–B3.6). Subfraction B3.4 (2 g) was purified on a C18 column (MeOH/H_2O, 15:85 → 23:77, v/v) to afford five subfractions, from which B3.4.2 gave **G-12** (12 mg) by preparative LC (ACN/H_2O, 20:80, v/v), and B3.4.4 afforded **G-15** (16 mg) and **G-11** (13 mg) after Sephadex LH-20 chromatography (MeOH). Fraction B5 (1.8 g) was separated on a C18 column with a MeOH/H_2O gradient (10:90 → 100:0, v/v) to obtain four subfractions (B5.1–B5.4). Subfraction B5.1 (130 mg) was crystallized from MeOH to yield **G-6** (25 mg). Fraction B6 (2.1 g) was chromatographed on a C18 column (MeOH/H_2O, 10:90 → 80:20, v/v), giving eight subfractions (B6.1–B6.8). Subfraction B6.1 yielded **G-17** (19 mg) after preparative LC (ACN/H_2O, 15:85, v/v), while B6.2 produced **G-1** (97 mg) after Sephadex LH-20 purification with MeOH.

2.2.3. Determination of the Chemical Structures

The chemical structures of the isolated compounds were elucidated using spectroscopic techniques, including mass spectrometry (MS), nuclear magnetic resonance (NMR), infrared spectroscopy (IR), and ultraviolet spectroscopy (UV).

2.2.4. α-Glu Inhibitory Activity Assay

The inhibitor assay of *α*-Glu was performed using the following reported by To et al. (2021) with slight modifications. In brief, 50 µL of *α*-Glu solution (0.2 U/mL) was pre-incubated with 50 µL of compounds (dissolved in DMSO) at 37ºC for 10 min. Subsequently, *p*-NPG (5 mM, 50 µL) substrate solution was added and incubated at 37oC for 20 min after the mixture vortexed. The reaction was terminated by adding 50 µL of 0.1 M Na_2CO_3. The absorbance of released p-nitrophenol (*p*-PNP) was measured at 405 nm using a microplate reader. All experiments were performed in triplicate.

2.2.5. XO Inhibitory Activity Assay

The XO inhibitory assay was evaluated using a slightly modified version of a previously reported method. The assay was performed by preparing a reaction mixture consisting of 200 µL of the test sample at varying concentrations (initially dissolved in DMSO (Merck) and then diluted to the desired concentration range, ensuring the final DMSO concentration did not exceed 2.5%), 50 µL of XO (Sigma, bovine milk origin, 0.2 U/mL), and 950 µL of sodium phosphate buffer (50 mM, pH 7.5). After incubation at 25°C for 15 min, 400 µL of 1.5 mM xanthine (Sigma) was added, followed by an additional 30 min incubation at the same temperature. The absorbance was measured spectrophotometrically at 295 nm. All experiments were conducted in triplicate, and the inhibition percentage was calculated. The IC_{50} values were derived from the inhibition data.

2.2.6. Network Pharmacology Analysis

The analytical procedure comprised the following steps: screening of bioactive constituents from *Glinus oppositifolius* and identification of their corresponding target proteins; construction of a compound–target interaction network; development of a protein–protein interaction (PPI) network for the potential targets; and functional enrichment analysis, including Gene Ontology (GO) annotation and Kyoto Encyclopedia of Genes and Genomes (KEGG) pathway analysis.

2.2.7. *Molecular Docking Analysis*

Molecular docking was conducted using AutoDock Vina 1.1.2. The 3D crystal structures of target proteins were obtained from the RCSB Protein Data Bank, and co-crystallized ligands were separated using Discovery Studio 2024. Water molecules were removed, polar hydrogens added, and Kollman charges assigned with AutoDock Tools 1.5.7.

Ligand structures were retrieved from PubChem or drawn manually, energy-minimized in Chem3D 19.0, and converted to .pdb and then .pdbqt formats using PyMOL 3.0.4 and AutoDock Tools 1.5.7. Docking results were assessed based on binding energy values (kcal/mol).

CHAPTER 3. RESULTS AND DISCUSSION

3.1. Bioactivity Assays of Extract Fractions

3.1.1. Inhibitory Activity of Extract Fractions Against α-Glucosidase

Table 3.1 Inhibitory activity of *Glinus oppositifolius* extract fractions against α-glucosidase

Sample	IC_{50} (μg/mL)

70% Ethanol extract	448,55 ± 1,86
EtOAc extract	105,10 ± 1,56
BuOH extract	484,99 ± 4,47
Acarbose	659,46 ± 6,97

3.1.2. Inhibitory Activity of Extract Fractions Against Xanthine Oxidase

Table 3.2. Inhibitory activity of *Glinus oppositifolius* extract fractions against xanthine oxidase

Sample	IC_{50} (µg/mL)
70% Ethanol extract	130,56 ± 3,79
EtOAc extract	29,67 ± 1,02
BuOH extract	83,16 ± 0,27
Allopurinol	0,52 ± 0,02

The 70% ethanol extract and its derived fractions exhibited inhibitory effects against both *α*-glucosidase and xanthine oxidase. Among them, the ethyl acetate (EtOAc) extract demonstrated the strongest inhibitory activity. Consequently, this fraction was selected for further isolation and evaluation of its bioactive constituents.

3.2. Structural Elucidation of the Isolated Compounds

3.2.1. Compound G-6: Apigenin-5-*O*-*β*-D-glucopyranosyl-8-*C*-*β*-D- glucopyranosid (a new compound)

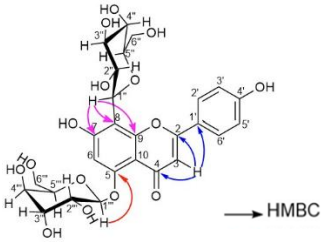

Figure 3.8. Chemical structure and HMBC correlations of **G-6**

Compound **G-6** was obtained as a yellow amorphous powder. Its UV spectrum in methanol exhibited absorption maxima at 268 nm and 338 nm, characteristic of a flavonoid chromophore. The IR spectrum displayed absorption bands at 3421 cm^{-1} (-OH), 1658 cm^{-1} (C=O), 1575 cm^{-1} (aromatic ring), and 1075 cm^{-1} (C–O–C). The molecular formula of **G-6** was determined to be $C_{27}H_{30}O_{15}$ based on the high-resolution negative ion electrospray mass spectrum ((-)-HR-ESI-MS), which showed a deprotonated molecular ion peak at m/z 593.1502 $[M–H]^-$ (calculated for $[C_{27}H_{29}O_{15}]^-$: 593.1512; Δ = –1.69 ppm).

The ^{13}C-NMR spectrum of **G-6** showed 27 carbon signals, including 15 in the aromatic region (δC 93–166), characteristic of a flavonoid skeleton. Signals at δC 60–80 and an anomeric carbon at δC 101.2 indicated two hexose units. The carbonyl carbon at δC 182.3 (C-4) and olefinic carbon at δC 102.5 (C-3, δH 6.86) confirmed a flavone nucleus, while the B-ring signals (δC 129.2, 115.9; δH 8.06, 6.90) identified the aglycone as apigenin. The ^{1}H-NMR spectrum showed two anomeric protons at δH 4.88 (J = 10.0 Hz) and 4.95 (J = 7.5 Hz), consistent with β-linked sugars. HSQC correlations with δC 73.3 and 101.2 suggested the coexistence of *C*- and *O*-glycosidic bonds. HMBC correlations of δH 4.95 ↔ δC 160.8 established an O-glycosidic linkage at C-5, while δH 4.88 ↔ δC 107.2, 155.0, and 161.2 confirmed a C-glycosidic bond at C-8. Thus, G-6 was identified as apigenin-5-*O*-*β*-D-glucopyranosyl-8-C-β-D-glucopyranoside, a new flavonoid glycoside from *Glinus oppositifolius.*

Table 3.8. NMR Spectroscopic Data of Compound **G-6**

G-6 (DMSO-d_6, 500 MHz)					
C	**δ_C (*ppm*)**	**δ_H (*ppm*) *J (Hz)***	***C***	**δ_C (*ppm*)**	**δ_H (*ppm*) *J (Hz)***
2	164,6	-	Glc-1''	73,3	4,88 *d* (*10,0)*
3	102,5	6,86 *s*	2''	71,7	3,72 *m*
4	182,3	-	3''	78,5	3,36 *m*
5	160,8	-	4''	70,7	3,38 *m*
6	98.5	6,61*s*	5''	81,9	3,28 *m*
7	161,2	-	6''	61,3	3,78 *m*; 3,54 *m*
8	107,2	-	Glc-1'''	101,2	4,95 *d (7,5*)
9	155,0	-	2'''	73,4	3,35 *m*
10	105,7	-	3'''	75,9	3,31 *m*
1'	121,1	-	4'''	69,5	3,21 *m*
2'	129,2	8,06 *d* (*9,0*)	5'''	77,1	3,41 *m*
3'	115,9	6,90 *d* (*9,0*)	6'''	60,6	3,70 *m;* 3,50 *m*
4'	161,7	-			
5'	116,2	6,96 *d* (*9,0*)			
6'	128,6	7,92 *d* (*9,0)*			

3.2.2. Compound G-11: Spergulin C (a new compound)

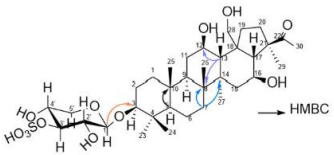

Figure 3.13. Chemical structure and HMBC correlations of **G-11**

Compound **G-11** was obtained as a white amorphous powder. The UV spectrum of **G-11** in methanol exhibited an absorption maximum at 203 nm. The IR spectrum showed characteristic absorption bands at 3480 cm^{-1} (-OH) and 1700 cm^{-1} (>C=O). The molecular formula of **G-11** was determined to be $C_{35}H_{58}O_{12}S$ based on high-resolution negative ion electrospray mass spectrometry ((-)-HR-ESI-MS), which showed a pseudo-

molecular ion peak at m/z 701.3567 $[M–H]^-$ (calculated for $[C_{35}H_{57}O_{12}S]^-$: 701.3576; Δ = –1.28 ppm).

The ^{13}C-NMR and DEPT spectra exhibited 35 carbon signals, including 30 from a triterpenoid aglycone and 5 from a pentose sugar. Key HMBC correlations (H-29/H-17/H-20 ↔ C-22; H-30 ↔ C-21) indicated a methyl ketone group at C-21. Deshielded protons at δH 3.26 (H-3), 4.22 (H-12), and 4.15 (H-16), with *δ*C 88.1, 69.7, and 64.4, confirmed hydroxyl groups at C-3, C-12, and C-16. These data identified a hopane-type aglycone bearing an acetyl and methyl group at C-21 and three hydroxyl groups at C-3, C-12, and C-16.

Compared with **G-9**, **G-11** lacked one methyl signal but displayed an additional oxymethylene at *δ*C 61.4; *δ*H 4.36 (H-28), correlated with H-17 (*δ*H 2.52), suggesting hydroxylation at C-28. The sugar moiety showed signals at *δ*C 106.3, 83.1, 73.6, 70.6, and 66.1, consistent with D-xylose, in which C-3′ is substituted by a –HSO_3 group. HMBC correlation between H-1′ and C-3 confirmed the *β*-D-xylose linkage at C-3 of the aglycone. COSY correlations further supported the proposed structure of **G-11.**

Table 3.13. NMR Spectroscopic Data of Compound **G-11**

G-11 (Pyridine-*d*$_5$,500MHz)					
C	***δ*$_C$ (*ppm*)**	***δ*$_H$ (*ppm*) *J* (*Hz*)**	***C***	***δ*$_C$ (*ppm*)**	***δ*$_H$ (*ppm*) *J* (*Hz*)**
1	38,5	0,84 *m*	19	46,1	1,9 *m*
2	26,5	1,8 *m*	20	37,8	1,83 *m* 2,09 *m*
3	88,1	3,26 *m*	21	52,8	-
4	39,3	-	22	214,4	-
5	55,3	0,68 *d* (10,7)	23	28,0	1,22 *s*

6	18,4	1,28 *m*	24	16,5	0,94 *s*
7	33,5	1,19 *m* 1,23 *m*	25	15,9	0,77 *s*
8	45,7	-	26	17,1	1,00 *s*
9	49,2	1,41 *m*	27	19,4	1,39 *s*
10	36,7	-	28	61,4	4,36 *d (10,8)*
11	31,5	2,07 *m*	29	21,1	1,69 *s*
12	69,7	4,22 *m*	30	26,0	2,36 *s*
13	56,6	1,87 *d (11,0)*	Xyl-1'	106,3	4,92 *d (7,0)*
14	41,9	-	2'	73,6	4,02 *m*
15	45,5	1,74 *m*	3'	83,1	5,40 *m*
16	64,4	4,15 *m*	4'	70,6	4,7 *m*
17	63,2	2,52 *d (11,5)*	5'	66,1	4,23 *m*
18	52,6	-			

3.2.3. Compound G-17: L-(-)-(N-*cis*-cinnamoyl)-arginin (a new compound)

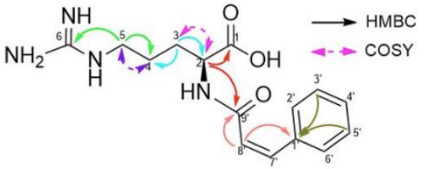

Figure 3.19. Chemical structure and HMBC correlations of **G-17**

Compound **G-17** was obtained as an amorphous yellow powder with UV absorption at 256 nm. Its IR spectrum showed bands for N–H (3348, 3119 cm^{-1}), C=O (1681 cm^{-1}), and aromatic C=N/C=C (1608–1450 cm^{-1}). HR-ESI-MS gave ion peaks at m/z 303.1442 $[M–H]^-$ and 305.1597 $[M+H]^+$, consistent with the formula $C_{15}H_{20}N_4O_3$.

The ^{1}H-NMR spectrum exhibited five aromatic protons (δH 7.27–7.47) and two olefinic protons (*δ*H 6.77, 6.08; J = 12.5 Hz), indicating a cis-cinnamoyl moiety, confirmed by COSY and HMBC correlations. The ^{13}C-NMR data showed 13 carbons, including nine from the cinnamoyl group and six

characteristic of an arginine residue (three methylenes, one methine, two quaternary carbons). COSY and HMBC correlations supported the arginine skeleton, and a cross-peak between H-2 (δH 4.29) and C-9′ (δC 169.1) indicated cinnamoyl substitution at the α-amino group.

The specific rotation $[\alpha]^{D27}$ = –16.7° confirmed an (S)-configuration at C-2. Comparison with literature data identified **G-17** as *L*-(–)-(*N*-cis-cinnamoyl)-arginine.

Table 3.19. NMR Spectroscopic Data of Compound **G-17**

G-17 ***(CH₃OH-d₆, 500 MHz)***					
C	***δ*C (*ppm*)**	***δH (ppm) J (Hz)***	**C**	***δ*C (*ppm*)**	***δH (ppm) J (Hz)***
Amino acid			cinnamoyl		
1	178,1		1’	136,8	-
2	55,3	4,31 t (6,5)	2’, 6’	130,2	7,49 *d (9,0)*
3	30,9	1,83 *m* 1,71 *m*	3’, 5’	129,3	7,29 *m*
4	26,1	1,52 *m*	4’	129,5	7,29 *m*
5	42,1	3,15 *m*	7’	138,0	6,79 *d (12,5)*
6	158,6	-	8’	125,1	6,09 *d (12,5)*
2-NH			9’	169,1	-

By combining and analyzing data from HR-MS and NMR spectra, the structures of twenty compounds (**G-1** → **G-20**) were elucidated. Among them, three compounds were identified as new natural products: G-6 (Apigenin-5-*O*-*β*-D-glucopyranosyl-8-*C*-*β*-D-glucopyranoside), G-11 (unidentified here), and **G-17** (*L*-(–)-(*N*-*cis*-cinnamoyl)-arginine). In addition, one compound was reported for the first time in this plant species, **G-20** (7-*O*-methylwogonin), while sixteen compounds were known compounds, including **G-1** (vicenin-2), **G-2** (spergulacin), **G-3** (glinoside C), **G-4** (spergulacin A), **G-5**

(spergulin B), **G-7** (trifolin), **G-8** (3-*O*-*β*-D-xylopyranosyl-spergulagenin A), **G-9** (spergulin A), **G-10** (vitexin), **G-12** (2″-p-coumaroylvitexin 7-glucoside), **G-13** (kaempferol), **G-14** (apigenin), **G-15** (astragalin), **G-16** (vanillin), **G-18** (cinnamic acid), and **G-19** (*trans*-ferulic acid).

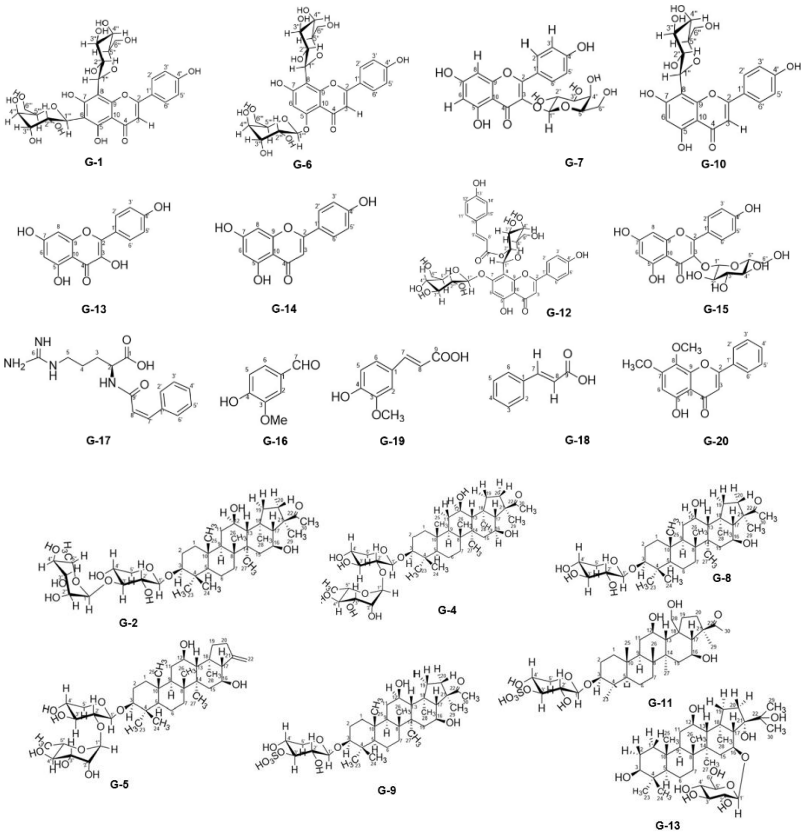

Figure 3.39. Chemical structure of **G-1→G-20**

3.3. Biological Activity Evaluation of the Isolated Compounds

3.3.1. Inhibitory Activity of the Isolated Compounds Against *α*-Glucosidase Enzyme

Table 3.23. Inhibitory activity of α-glucosidase enzyme by the compounds isolated from *Glinus oppositifolius* (L.) A. DC.

Sample	IC_{50} (μM)	Sample	IC_{50} (μM)
G-1	1247,21 ± 2,15	**G-12**	222,22 ± 3,71
G-2	310,51 ± 1,38	**G-13**	9,52 ± 0,19
G-3	ND	**G-14**	10,28 ± 0,05
G-4	ND	**G-15**	80,27 ± 1,50
G-5	ND	**G-16**	ND
G-6	257,90 ± 1,00	**G-17**	ND
G-7	380,71 ± 5,43	**G-18**	ND
G-8	13,99 ± 0,33	**G-19**	ND
G-9	ND	**G-20**	94,92 ± 1,85
G-10	193,60 ± 2,47	**Acarbose**	1021,47 ± 10,79
G-11	31,23 ± 0,45		

ND: not detected (no inhibitory activity observed)

Among the 20 isolated compounds, **G-8**, **G-11**, **G-13**, **G-14**, **G-15**, and **G-20** exhibited strong inhibitory activity against *α*-glucosidase, with IC_{50} values ranging from 9.52 to 94.92 μM. Among these, compound **G-13** (IC_{50} = 9.52 ± 0.19 μM) showed the most potent inhibitory effect. Compounds **G-10**, **G-2**, **G-6**, and **G-7** demonstrated moderate to weak inhibition, with IC_{50} values ranging from 193.60 to 380.71 μM. Compound **G-1** displayed the weakest activity, with an IC_{50} value of 1247.21 ± 2.15 μM. The remaining compounds exhibited no detectable *α*-glucosidase inhibitory activity.

3.3.2. Inhibitory Activity of the Isolated Compounds Against Xanthine Oxidase

Table 3.24. Inhibitory activity of xanthine oxidase enzyme by the compounds isolated from *Glinus oppositifolius* (L.) A. DC.

Sample	IC_{50} (μM)	Sample	IC_{50} (μM)
G-1	56,82 ± 1,95	**G-12**	127,51 ± 2,33
G-2	288,68 ± 1,94	**G-13**	26,18 ± 0,78
G-3	ND	**G-14**	10,26 ± 0,55
G-4	ND	**G-15**	144,65 ± 0,17
G-5	ND	**G-16**	5,37 ± 0,33
G-6	ND	**G-17**	178,02 ± 1,65
G-7	ND	**G-18**	106,69 ± 3,55
G-8	ND	**G-19**	87,40 ± 1,96
G-9	394,42 ± 1,35	**G-20**	ND
G-10	927,49 ± 4,48	**Allopurinol**	3,84 ± 0,11
G-11	ND		

ND: not detected (no inhibitory activity observed)

Among the 20 isolated compounds, **G-1, G-13, G-14, G-16**, and **G-19** exhibited strong inhibitory effects on xanthine oxidase, with IC_{50} values ranging from 5.37 to 87.40 μM. Notably, compound **G-16** (IC_{50} = 5.37 ± 0.33 μM) demonstrated the most potent inhibition. Compounds **G-2, G-9, G-10, G-12, G-15, G-17**, and **G-18** showed weaker inhibitory activity, with IC_{50} values between 106.69 and 394.42 μM. Compound **G-10** exhibited the weakest inhibition, with an IC_{50} value of 927.49 ± 4.48 μM. The remaining compounds did not display detectable xanthine oxidase inhibitory activity.

3.4. Prediction of Mechanisms of Action and Key Bioactive Compounds in the Treatment of Type 2 Diabetes Mellitus

3.4.1. Compound Screening and Construction of the Compound–Target Network

Based on UPLC–HRMS analysis and experimental data, a total of 43 compounds were identified from Glinus oppositifolius. After applying the Lipinski's Rule of Five for screening, 34 compounds were selected as pharmacologically active

candidates. Using the SwissTargetPrediction platform, 831 potential targets were predicted for these 34 compounds. When compared with 2,446 diabetes-related targets collected from GeneCards and OMIM, 326 overlapping targets were identified as potential therapeutic targets.A compound–target interaction network was subsequently constructed, comprising 360 nodes and 1,545 edges, representing the interactions between compounds and their targets. The three compounds with the highest degree of centrality in the network were identified as: 3-oxo-olean-12-ene-28,30-dioic acid, 6,8-dimethyl-5,7,4′-trihydroxyflavone, and 7-hydroxy-5-methoxy-6,8-dimethylflavone.

3.4.2. Construction of the Protein–Protein Interaction Network

From the 326 predicted targets, a Protein–Protein Interaction (PPI) network was constructed using the STRING database with a high confidence threshold. The resulting network consisted of 326 nodes (representing proteins) and 7,297 edges (representing protein–protein interactions). This network was analyzed using Cytoscape 3.10.2 and the CytoNCA plugin. Based on centrality parameters (Degree Centrality [DC] > 100, Betweenness Centrality [BC] > 0.0049, Closeness Centrality [CC] > 0.59), 28 core proteins were identified to construct a refined PPI subnetwork containing 374 edges. Prominent hub proteins included AKT1, TNF, IL6, ALB, TP53, SRC, EGFR, STAT3, and PPARG, which are considered key molecular targets mediating the pharmacological effects of *Glinus oppositifolius.*

3.4.3. Gene Ontology Functional Enrichment Analysis (GO)

GO enrichment analysis of the 326 potential targets was performed and classified into three main categories: Biological Process (BP): response to chemical stimulus, response to oxygen-containing compounds, and response to external stimuli. Cellular Component (CC): membrane microdomain and receptor complex. Molecular Function (MF): protein tyrosine kinase receptor activity and nuclear receptor activity.

3.4.4. KEGG Pathway Enrichment Analysis

KEGG pathway analysis identified 239 significantly enriched signaling pathways (FDR < 0.05). The five most relevant pathways were: EGFR tyrosine kinase inhibitor resistance (hsa01521), Prostate cancer, AGE–RAGE signaling pathway in diabetic complications, Endocrine resistance, and HIF-1 signaling pathway. These pathways are primarily associated with insulin resistance, inflammation, and oxidative stress, which are major pathogenic mechanisms underlying Type 2 Diabetes Mellitus (T2DM).

3.4.5. Molecular Docking Analysis

Molecular docking simulations were performed between the three key bioactive compounds and nine core protein targets to validate their binding affinities. The docking protocol was considered reliable, with RMSD values ranging from 0.835 to 1.244 Å (< 2 Å). The strongest binding interactions were observed as follows: 3-oxo-olean-12-ene-28,30-dioic acid – ALB: −10.1 kcal/mol; 7-hydroxy-5-methoxy-6,8-dimethylflavone – TNF: −9.9 kcal/mol; 3-oxo-olean-12-ene-28,30-dioic acid – SRC: −9.4 kcal/mol. These results further

corroborate the network pharmacology findings and confirm the reliability of the predicted molecular targets of *Glinus oppositifolius* in the management of Type 2 Diabetes Mellitus.

3.5. Prediction of Mechanisms of Action and Key Bioactive Compounds in the Treatment of Gout

3.5.1. Compound Screening and Construction of the Compound–Target Network

By cross-referencing with 1,260 gout-related targets (collected from GeneCards and OMIM databases), a total of 149 overlapping targets were identified as potential therapeutic targets. The compound–target interaction network was subsequently constructed, consisting of 183 nodes and 751 edges, representing the interactions between bioactive compounds and their predicted targets. The three compounds exhibiting the highest degree of centrality in the network were: trans-Ferulic acid, 7-hydroxy-5-methoxy-6,8-dimethylflavone, and Lutein.

3.5.2. PPI Construction of the Protein–Protein Interaction Network

From the 149 potential targets, a Protein–Protein Interaction (PPI) network was established using the STRING database. After excluding three non-interacting targets (GLRA2, PLAA, and GLRA1), the resulting network comprised 146 nodes and 1,808 edges. Subsequent filtering based on centrality criteria (DC > 40, BC > 0.0029, CC > 0.5513) yielded a refined PPI subnetwork consisting of 22 nodes and 218 edges. The core hub proteins identified were IL6, ALB, TNF, TP53, and SRC,

which play crucial roles in inflammation, oxidative stress, and immune response regulation associated with gout pathogenesis.

3.5.3. Gene Ontology Functional Enrichment Analysis (GO)

GO enrichment analysis of the 146 potential targets classified them into three main categories: Biological Process (BP): response to oxygen-containing compounds, cellular response to chemical stimuli, and response to organic substances. Cellular Component (CC): receptor complex, plasma membrane, and lateral plasma membrane. Molecular Function (MF): small molecule binding and protein tyrosine kinase activity.

3.5.4. KEGG Pathway Enrichment Analysis

KEGG pathway analysis identified 200 significantly enriched pathways (FDR < 0.05). The three most relevant pathways were: Pathways in cancer (hsa05200), Lipid and atherosclerosis (hsa05417), and PI3K–Akt signaling pathway (hsa04151).

These pathways are closely associated with chronic inflammation, lipid metabolism disorders, and uric acid metabolism, which represent the major pathogenic mechanisms of gout.

3.5.5. Molecular Docking Analysis

Molecular docking was conducted between the three key compounds and five core protein targets to validate their binding affinities. The strongest binding interactions were observed as follows: 7-hydroxy-5-methoxy-6,8-dimethylflavone –TNF: −9.9 kcal/mol; 7-hydroxy-5-methoxy-6,8-dimethylflavone – SRC: −9.3 kcal/mol; Lutein – SRC: −8.5 kcal/mol. These findings reinforce the network pharmacology results and confirm the reliability of the predicted target

interactions, highlighting the potential mechanisms through which *Glinus oppositifolius* may exert therapeutic effects in gout treatment.

CHAPTER 4. CONCLUSIONS AND RECOMMENDATIONS

This study yielded the following key findings: From the aerial parts of *Glinus oppositifolius*, 20 compounds (**G-1 → G-20**) were isolated and identified, including 9 flavonoids, 7 saponins, and 4 other compounds. Among the solvent extracts, the ethyl acetate fraction showed the strongest inhibitory activity against both *α*-glucosidase and xanthine oxidase.

Five compounds **G-1, G-13**, **G-14**, **G-16**, and **G-19** exhibited potent xanthine oxidase inhibition with IC_{50} values of 5.37–87.40 μM. Network pharmacology and molecular docking analyses indicated that *G. oppositifolius* may exert antidiabetic effects by improving insulin resistance, preventing diabetic complications, and providing anti-inflammatory and antioxidant benefits. Similarly, these analyses suggested antigout potential through anti-inflammatory, antioxidant, uric acid–lowering, and lipid-regulating mechanisms, thereby reducing cardiovascular risks.

NEW CONTRIBUTIONS OF THE THESIS

- This study represents the first report on the xanthine oxidase inhibitory activity of *Glinus oppositifolius*.
- Three new compounds were isolated and structurally characterized from the aerial parts of *G. oppositifolius*: Apigenin-5-*O*-*β*-D-glucopyranosyl-8-*C*-*β*-D-glucopyranoside, Spergulin C, *L*-(-)-(*N*-*cis*-cinnamoyl)-arginine. Their *α*-glucosidase and xanthine oxidase inhibitory activities were

evaluated for the first time. The compound 7–*O*–methylwogonin was isolated for the first time from the aerial parts of *G.oppositifolius*, and this study is also the first to report its inhibitory effects on α-glucosidase and xanthine oxidase.

- This is the first investigation applying network pharmacology to explore bioactive compounds and potential molecular mechanisms of *Glinus oppositifolius* in the treatment of type 2 diabetes mellitus and gout, providing a scientific basis for further pharmacological and therapeutic studies.